Global Mirror Modes in the Magnetosheath

Jay R. Johnson and C. Z. Cheng

Princeton Plasma Physics Laboratory, Princeton, NJ 08543

Abstract

A global stability analysis of mirror modes in the magnetosheath is presented. The analysis is based upon the kinetic-MHD formulation which includes relevant kinetic effects such as Landau resonance and gradient drift effects related to inhomogeneities in the background density, temperature, pressure and its anisotropy, magnetic field, and plasma flow velocity. Pressure anisotropy provides the free energy for the global mirror mode. The local theory of mirror modes predicts purely growing modes confined in the unstable magnetosheath region; however, the nonlocal theory that includes the effects of gradients and plasma flow predicts modes with real frequencies which propagate with the flow from the magnetosheath toward the magnetopause boundary. The real frequency is on the order of a combination of the diamagnetic drift frequency and the Doppler shift frequency associated with plasma flow. The diamagnetic drift frequency provides a wave phase velocity in the direction of the magnetopause so that wave energy accumulates against the magnetopause boundary, and the amplitude is skewed in that direction. On the other hand, plasma flow also gives rise to a real phase velocity, but the phase velocity is smaller than the flow velocity. As a result, the wave amplitude is increased in the wake of the plasma flow and piles up against the bow shock boundary.

I. INTRODUCTION

Recently much attention has been given to the identification of wave modes in the magnetosheath and, in particular, near the magnetopause [1–8]. Such efforts are of interest primarily because the identified modes may grow to substantial amplitudes and can cause significant change in plasma profiles and pressure anisotropy. For example, it is thought that ion-cyclotron waves control the degree of pressure anisotropy in the magnetosheath [9]. Moreover, low frequency MHD waves such as mirror modes excited in the magnetosheath or fast compressional Alfvén waves originating from the bow shock can propagate to the magnetopause and lead to significant plasma transport. Transport at the magnetopause due to low frequency MHD wave turbulence can be very efficient because magnetic field and density gradients at the magnetopause efficiently couple large scale wave energy into small scale kinetic Alfvén waves with perpendicular wavelength on the order of the gyroradius [10–13]. Using quasilinear theory we have shown that these waves can lead to efficient particle transport across the magnetic field for both northward and southward IMF. Moreover, for southward IMF, we have shown that kinetic Alfvén waves can propagate to the location because the Landau damping is suppressed by magnetic gradient and curvature drifts [12]. As a consequence, magnetic islands can form and for a typical spectrum of low frequency MHD waves, there will be multiple overlapping islands in the particle phase space which can lead to massive particle transport.

The mirror modes destabilized in the magnetosheath are of substantial interest they can couple a significant amount of wave energy from the magnetosheath to waves at the magnetopause. The mirror modes are unstable and can grow to large amplitudes because the magnetosheath is characterized by a large pressure anisotropy [14, 15]. Based on local mirror mode theory the mirror modes is purely growing and has no real frequency so as a consequence they would be confined in the magnetosheath and can not propagate to the magnetopause. In this work we shall study the nonlocal effects of realistic background gradients and plasma flow and demonstrate that the mode frequency is actually complex with

a substantial real component due to particle diamagnetic drift and Doppler shift associated with plasma flow. With a substantial real frequency, these modes can propagate to the magnetopause and efficiently mode convert into kinetic Alfvén waves which may play an important role in transport processes at the magnetopause.

Large pressure anisotropy develops in the magnetosheath because as plasma crosses the bow shock, the flow velocity perpendicular to the magnetic field is converted into into gyromotion yielding a large perpendicular plasma temperature. Motion along the magnetic field is not readily converted into thermal energy so that a large anisotropy develops with $\beta_\perp > \beta_{||}$. In the magnetosheath the kinetic pressure dominates the relatively weak magnetic field so that typically $\beta > 1$. For such conditions the plasma is unstable to the well known mirror mode [1, 3, 16]. Near the magnetopause, the magnetic field sharply increases while the plasma pressure decreases and becomes more isotropic. The plasma β falls to a more typical magnetospheric value much less than 1 which suppresses the mirror mode instability.

Kinetic effects on waves at the magnetopause have been extensively studied using Vlasov theory based upon a homogeneous background [2, 3, 9, 17–19]. While these calculations provide very useful information about local threshold conditions, they do not account for kinetic effects that involve background gradients and boundary conditions. On the other hand, MHD wave analysis effectively deals with complicated boundary conditions and global gradients, but fails to account for important kinetic effects.

While one- and two-dimensional hybrid simulations [8] have the advantage of describing many kinetic effects of ion, it is difficult to prescribe and maintain an realistic equilibrium magnetic field geometry with appropriate boundary conditions. Moreover, the extension of such models to include the important effects of curvature is not straightforward. We employ the kinetic-MHD approach which is an attempt to incorporate the most important ion kinetic effects into the MHD formalism [20, 21]. The gyrokinetic equation, which is essentially the gyroaveraged Vlasov equation, is the cornerstone of the model. Moments of the gyrokinetic equation are taken and provide a modified momentum equation and Ohm's law. This approach retains the important kinetic effects of Landau damping and gradient

drift as well as the physics associated with the ion magnetic gradient and curvature drifts. Moreover, it is straightforward to generalized this model to realistic two or three dimensional equilibrium profiles.

The organization of this paper is as follows. We shall briefly review the mirror mode and point out the important consequences introduced by (a) background gradients in the equilibrium and (b) kinetic effects. We present the kinetic-MHD model for the mirror mode which includes these effects. Then, we solve for the global mirror eigenmodes using a one-dimensional equilibrium based upon typical observations and interpret the results. Finally, a conclusion and discussion is given.

II. BACKGROUND GRADIENT AND KINETIC EFFECTS ON MIRROR MODES

Without kinetic effects, low-frequency ($\omega \ll k_{||}v_A, k_{||}c_s$) compressional magnetic field fluctuations may be described by the MHD equation

$$\left(\frac{\partial}{\partial t} + \mathbf{V}_0 \cdot \nabla\right)^2 \mathbf{B} \cdot \delta\mathbf{B} = \mathbf{B} \cdot \nabla \left(\frac{\sigma}{B^2}\mathbf{B} \cdot \nabla\mathbf{B} \cdot \delta\mathbf{B}\right) + \nabla_\perp^2 \left(\tau_{MHD}\mathbf{B} \cdot \delta\mathbf{B}\right) \tag{1}$$

where the firehose and mirror instability parameters are respectively

$$\sigma = 1 + (\beta_\perp - \beta_{||})/2 \tag{2}$$

and

$$\tau_{MHD} = 1 + \beta_\perp(1 - \beta_\perp/\beta_{||}). \tag{3}$$

The dispersion relation for waves without background flow is $\omega^2 = \sigma k_{||}^2 v_A^2 + \tau_{MHD} k_\perp^2 v_A^2$ which reduces in the isotropic limit, $\sigma, \tau \to 1$, to the well known compressional Alfvén wave. In a plasma with $\beta_\perp > \beta_{||} \sim 1$, $\tau_{MHD} < 0$ can lead to the well known purely growing mirror instability.

Modifications to the simplistic uniform plasma MHD description of the compressional wave can be significant. In the magnetosheath and near the magnetopause it is important to

consider the effects of gradients in the equilibrium as well as kinetic effects. The parameter, τ_{MHD}, which indicates regions of local instability when negative, has a profile which changes from positive in the solar wind (relatively isotropic) to negative in the magnetosheath (due to large pressure anisotropy) to positive in the magnetosphere (low β, less anisotropy). As a consequence, (1) describes an eigenmode with a specific eigenfrequency localized in the region of instability. Moreover, as the instability grows, wave energy is transported out of the region of instability. The global solution gives information about how energy from this instability may be transported from the magnetosheath across magnetopause.

The background plasma flow is also important. In a uniform plasma, the mirror mode is purely growing in the plasma frame and should be convected with the flow. However, if the background plasma flow is nonuniform, deceleration of plasma can lead to wave pile up and modify the wave structure. Furthermore, purely growing modes can acquire a real frequency due to Doppler shift.

If kinetic effects are included in Eq. (1), kinetic contributions arise which modify the term proportional to τ_{MHD} so that τ_{MHD} must be replaced by an appropriate kinetic τ which contains wave-particle resonances and finite Larmor radius effects. In the low frequency limit ($\omega \ll k_{\|} v_{th\|}$), the kinetic τ reduces to τ_{MHD}. It has already been shown that kinetic effects strongly affect the MHD picture of the mirror instability. If ($\omega \sim k_{\|} v_{th\|}$), then wave particle resonance is important. Hasegawa [16] first provided a description of kinetic effects on the mirror mode. More recently extensive studies of local mirror mode theories including kinetic effects have been compiled [1–3, 9, 17–19]. Southwood [22] has provided an excellent physical picture of the kinetic effects on the instability and relates the instability to resonant particles with zero phase velocity. An important feature of the kinetic dispersion relation is that for an anisotropic plasma, in addition to the weakly damped fast magnetosonic wave found in the limit $\omega \gg k_{\|} v_{th\|}$, the mirror mode is found with $\omega \ll k_{\|} v_{th\|}$. For low frequencies ($\omega \ll k_{\|} v_{th\|}$), the mirror mode is well approximated by the MHD description and as such, the threshold condition for the kinetic mirror mode remains the same although growth rates are significantly reduced when $\omega \sim k_{\|} v_{th\|}$.

Other kinetic effects not described by uniform plasma Vlasov theory also arise where gradients are important. Hasegawa first described these effects as the drift-mirror mode [16], but these effects were thought to be unimportant because local gradients in the magnetosheath are generally small; however, we shall show that large localized gradients at the magnetopause can affect the global structure and provide a real frequency to the mirror mode. The gradients enter into the kinetic description through the diamagnetic drift. At the magnetopause, the diamagnetic drift frequency, $\omega_* \sim k_\| v_{thi} \rho_i / L_{MP}$ (L_{MP} is the gradient scale at the magnetopause, $k_\|$ is the azimuthal wave number, v_{thi} is the ion thermal velocity, and ρ_i is the ion gyroradius) can be significant and for typical magnetopause parameters, $\omega_* \sim k_\| v_A$.

III. KINETIC-MHD FORMULATION OF THE MIRROR MODE

An appropriate description of the mirror mode in the magnetosheath and near the magnetopause should attempt to account for the effects outlined in the last section. In particular, the model should contain the global profile effects which arise for inhomogeneous flow velocity, density, pressure, temperature, and magnetic field. Moreover, the model should contain important kinetic effects associated with the wave-particle interaction and diamagnetic drift. The kinetic-MHD model, which retains all of these effects is appropriate because the smallest background scale (the magnetopause) is typically the order of 10 ρ_i and thus satisfies the gyrokinetic approximation. To focus on the effects described above, we take for simplicity a one-dimensional equilibrium in the x direction which is taken to be normal to the magnetopause. While we expect that the two-dimensional and three-dimensional nature of the magnetopause can be important, the one-dimensional equilibrium gives us an abundance of new insight on the mirror mode. All equilibrium quantities will be functions of x only. For simplicity, we take the magnetic field and velocity to be $B_0(x)\hat{z}$ and $V_0(x)\hat{x}$ respectively. We neglect drifts due to magnetic field gradients and curvature in the resonant wave-particle interaction (which at most will shift the real frequency of the modes by a negligible amount).

Coupling to transverse magnetic fluctuations is ignored. If $\omega < k_{||}c_s, k_{||}v_A$ this assumption is reasonable, but we expect that there will be localized coupling near the location where the phase velocity of the wave approaches v_A or c_s leading to mode conversion to kinetic Alfvén waves or damping from the sound continuum.

The kinetic-MHD equations then reduce to Eq. (1) with kinetic modifications to the instability parameter,

$$\tau_{MHD}\mathbf{B}\cdot\delta\mathbf{B} \rightarrow \tau\mathbf{B}\cdot\delta\mathbf{B} \equiv \tau_{MHD}\mathbf{B}\cdot\delta\mathbf{B} + \delta\hat{p}_\perp, \tag{4}$$

which arise through the nonadiabatic pressure response,

$$\delta\hat{p}_\perp = m\int d^3v(\mathbf{v}_\perp - \mathbf{V_0})^2 g/2. \tag{5}$$

The nonadiabatic particle distribution, g, evolves according to

$$(\omega - i\mathbf{v}_{||}\cdot\nabla - i\mathbf{V_0}\cdot\nabla)g = -\frac{q}{m}\frac{\partial F}{\partial\mathcal{E}}\left(1-\frac{\omega_*}{\omega}\right)\frac{\omega v_\perp}{k_\perp}J_1(k_\perp v_\perp/\Omega)\frac{\mathbf{B}\cdot\delta\mathbf{B}}{B} \tag{6}$$

where it is implicitly understood that $k_\perp$ and ω_* are operators [23]. (We have dropped several terms in Eq. 6 which couple to the transverse magnetic field and parallel electric field through the magnetic gradient and curvature drifts which are smaller than the term proportional to $\delta B_{||}$ which contains the essential kinetic effects required to replicate the well known mirror mode dispersion relation [16].) Because $k_\perp\rho_i < 1$ we may formally expand the Bessel function to retain nonlocal effects in (6). We solve the integral equation using an expansion equivalent to a WKB approximation in the $\hat{\mathbf{x}}$ direction. We verify the validity of that approximation *a posteriori*. This approximation allows us to replace $\mathbf{V}_0\cdot\nabla g$ by $g\mathbf{V}_0\cdot\nabla\delta B_{||}/\delta B_{||}$.

We solve Eq. (1) with Eq. (4) using

$$\delta\hat{p} = -\frac{\beta_\perp T_\perp}{T_{||}}\Big((\zeta-\zeta_*^{(1)})Z(\zeta)2\mathcal{I}_3/\lambda - \zeta_*^{(2)}Z(\zeta)2\mathcal{I}_5/\lambda + \zeta_*^{(3)}\zeta(1+\zeta Z(\zeta))2\mathcal{I}_3/\lambda\Big)\,\mathbf{B}\cdot\delta\mathbf{B} \tag{7}$$

$$\zeta = \frac{(\omega - iV_0\cdot\nabla)}{\sqrt{2}k_{||}v_{th||}} \tag{8}$$

$$\zeta_*^{(1)} = \frac{\mathbf{B}\times\mathbf{k}_\perp v_{th\perp}}{\sqrt{2}k_\parallel v_{th\parallel}}\rho_i\left(\frac{\nabla n}{n}+\frac{1}{2}\frac{\nabla T_\parallel}{T_\parallel}-\frac{\nabla T_\perp}{T_\perp}\right) \tag{9}$$

$$\zeta_*^{(2)} = \frac{\mathbf{B}\times\mathbf{k}_\perp v_{th\perp}}{\sqrt{2}k_\parallel v_{th\parallel}}\rho_i\left(\frac{\nabla T_\perp}{T_\perp}\right) \tag{10}$$

$$\zeta_*^{(3)} = \frac{\mathbf{B}\times\mathbf{k}_\perp v_{th\parallel}}{\sqrt{2}k_\parallel v_{th\parallel}}\rho_i\left(\frac{\nabla T_\parallel}{T_\parallel}\right) \tag{11}$$

where $\lambda = k_\perp^2\rho_i^2/2$. The integral operators, $\mathcal{I}_3, \mathcal{I}_5$ are defined in the appendix and involve integrals over Bessel's functions. For small $k_\perp\rho_i$, $2\mathcal{I}_3/\lambda \sim 1$ and $2\mathcal{I}_5/\lambda \sim 3$. This set of equations properly reduces to the kinetic dispersion relation for $\zeta, \zeta_* \ll 1$:

$$\omega = \mathbf{k}\cdot\mathbf{V}_0 + \omega_* - ik_\parallel v_{th\parallel}\sqrt{\frac{2}{\pi}}\frac{T_\parallel}{\beta_\perp T_\perp}\left(\frac{\sigma k_\parallel^2}{k_\perp^2}+\tau_{MHD}\right) \tag{12}$$

where $\omega_* = (3\omega_{*p}-\omega_{*n})/2$ with $\omega_{*n} = -\rho_i v_{th\perp}\mathbf{b}\times\mathbf{k}\cdot\nabla n/n$ and $\omega_{*p} = -\rho_i v_{th\perp}\mathbf{b}\times\mathbf{k}\cdot\nabla P/P$.

Boundary conditions at the bow shock and magnetopause are critical in determining the structure of the modes. Because the group velocity of the modes that we consider are far less than the flow velocity in the solar wind, no wave information can be carried across the bow shock. This property is manifest in a singularity at the location where $\tau_{MHD} = (V_0/v_A)^2 = M_A^2$. At that location, the group velocity of compressional waves propagating against the flow approaches zero. A careful expansion of the MHD equations near this point indicates that the solution can consist of two Frobenius solutions, one of which is a power series and the other dominated by a logarithmic singularity. The behavior of the solutions is very similar to the behavior of MHD solutions near the well known field line resonance [24]. In this case, however, we choose the coefficient of the logarithmic solution to vanish because there is no physical mechanism which can provide the buildup of energy at the boundary. The remaining solution behaves like $c(1+\eta^2 x+...)$ where $\eta = \omega/\nabla V_0$ with $\eta \ll 1$ for a sharp boundary. In essence, this means that $d\delta B_\parallel/dx \approx 0$ near the boundary which can be interpreted as a reflecting boundary condition. The amplitude of the wave should reduce to zero in a small boundary layer near the bow shock when appropriate kinetic effects and coupling are include. We take the approximation $d\delta B_\parallel/dx \approx \eta^2$ near the bow

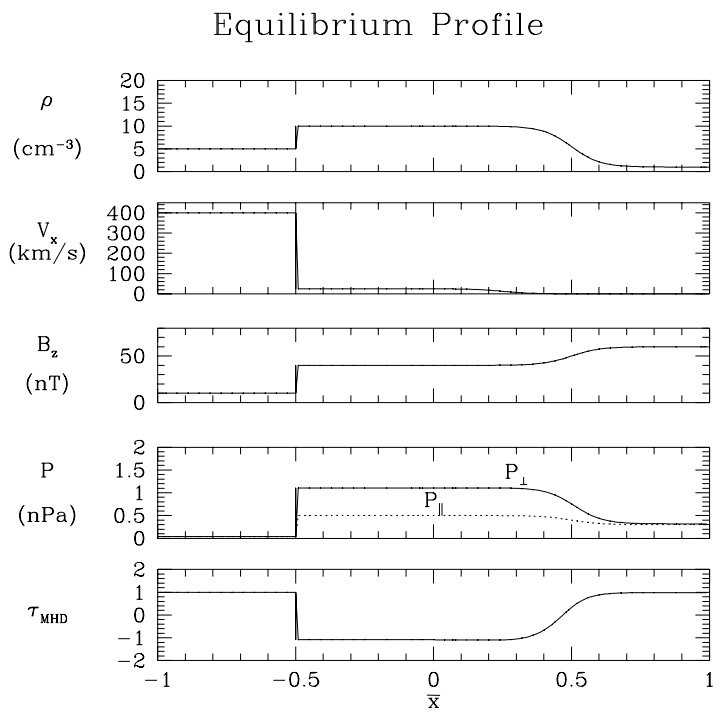

FIG. 1. Model steady state configuration for the global mode analysis for $\Delta = L_{MP}/L_\tau = 0.05$ and $M_A = V_0/v_{A0} = 0.1$ where v_{A0} is the Alfvén velocity at $\bar{x} = 0$. L_{MP} and L_τ are the width of the magnetopause and magnetosheath respectively.

shock in all of our results. On the magnetospheric side of the magnetopause we take the boundary condition that the solution connects to the appropriate exponentially decaying Eikonal solution which we obtain implicitly from the differential equation.

IV. RESULTS

We solve for the normal modes of the outlined system of equations for a steady state configuration based upon a typical pass through the magnetosheath and magnetopause [7,15]. In Fig. 1 we display typical steady state radial profiles for northward IMF. Although a true steady state configuration requires at least two dimensions in order to properly model the normal gradients in the plasma flow, the normal component of the bulk flow in the

magnetosheath is typically much smaller than the plasma and magnetic pressures and thus does not appreciably affect the gradients that enter though the plasma pressure and magnetic field and thus the essential MHD profiles do satisfy a steady state solution to first order in $\rho V_0^2/(P + B^2/2)$. On the other hand, the Doppler effects may be reasonably modeled by specifying a small normal velocity profile which is meant to be similar to what one would expect from a two dimensional steady state configuration. We introduce two spatial scales: L_τ is the scale length of the unstable region based upon $\tau_{MHD} < 0$ which corresponds roughly to the width of the magnetosheath ($\approx 2 - 5 R_E$ [25]), and L_{MP} represents the gradient scale length of the magnetopause ($\approx 10\rho_i$). The Mach number, M_A is given by the ratio V_0/v_{A0} where v_{A0} is the Alfvén velocity at $\bar{x} = 0$. The profile of $V_0$is chosen to decrease from the bow shock slowly to a value of zero at the magnetopause. The dimensionless radial coordinate is $\bar{x} = \pi x/L_\tau$. The bow shock is at $\bar{x} = -0.5$ and magnetopause at $\bar{x} = 0.5$. The dimensionless frequency is $\bar{\omega} = \omega L_\tau/\pi v_{A0}$. For typical parameters, this gives a frequency $f = (10-100)\bar{\omega}$ mHz. The wavevectors in the directions perpendicular to x remain constant. They are defined by k and θ where $k^2 = k_y^2 + k_z^2$ and $\theta = \tan^{-1}(k_y/k_z)$. The results displayed here have $k_0\pi/L_\tau = 5$ and $\theta = 30°$. For larger values of θ, the mode becomes more stable.

For a sharp magnetopause, there is a spectrum of purely growing modes up to an accumulation point. The boundary conditions limit the growth rate. For a smooth variance in the density, pressure and its anisotropy, and magnetic field, the kinetic part of τ has both a real and an imaginary part (which arises from the diamagnetic drift). The imaginary part of τ causes the eigenvalue to become complex rather than purely imaginary. If ω_* were uniform the real frequency is identically ω_*, but for nonuniform diamagnetic effects, the real frequency arises as an averaged ω_*. As the scale of the magnetopause is increased, the real frequency increases. The normal bulk plasma flow velocity also provides a significant contribution to the real frequency which is roughly given by an averaged $\mathbf{k} \cdot \mathbf{V}_0$. (Note that we have not included the $\hat{y}$ component of flow which would lead to a further Doppler shift in the real frequency.)

To illustrate these two effects we plot in Fig. 2 the evolution of the mode frequencies

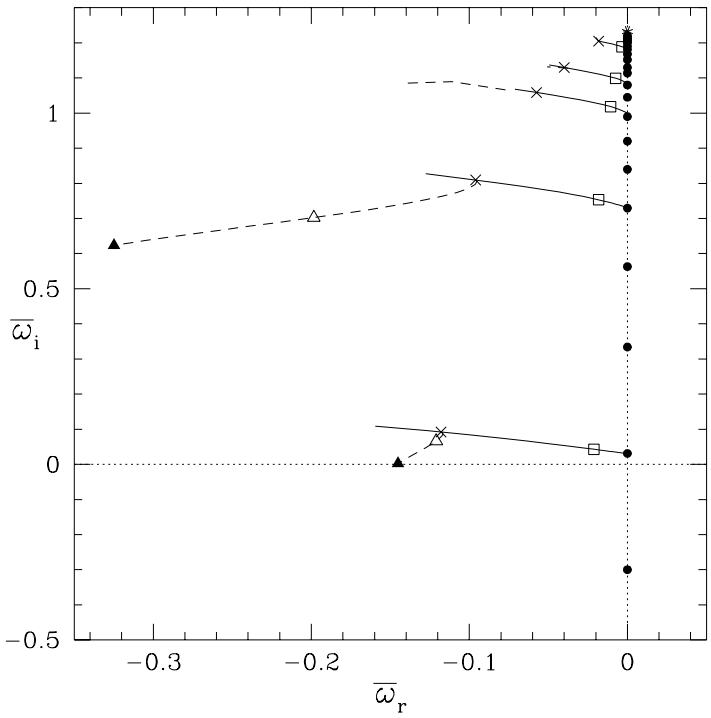

FIG. 2. Evolution of the eigenfrequencies ($\bar{\omega} = \omega L_\tau/\pi v_{A0}$) of the eigenfunctions. The solid lines correspond to evolution of the roots in Δ with $M_A = 0$. The dashed lines correspond to evolution of the roots in M_A with $\Delta = 0.05$. Various points on these curves are indicated by symbols described in Table 1.

as functions of the magnetopause gradient scale and the plasma flow, $\mathbf{V}_0$. Each curve in this figure corresponds to an eigenfunction with a specific number of nodes beginning with the damped fundamental in ascending order. In particular, we plot the evolution of the $n = 2, 5, 8, 10, 15$ modes, where n is the number of nodes in the radial wave function ($k_x \sim (n+1)\pi/L_\tau$). The solid curves show the evolution of the mode frequency as a function of $\Delta = L_{MP}/L_\tau$ with $\mathbf{V}_0 = 0$. The dashed curves show the evolution of modes as a function of M_A with $\Delta = 0.05$. Specific values of Δ and M_A are indicated by symbols described in Table 1.

Symbol	Δ	M_A
●	0	0
□	0.01	0
×	0.05	0
△	0.05	0.1
▲	0.05	0.2

TABLE I. Specific values of Δ and M_A are indicated by these symbols in Fig. 2.

As expected, for small L_{MP}, the modes all line up on the imaginary axis. However, as L_{MP} increases to more realistic values, the eigenvalues undergo excursions into the complex plane and are characterized by a significant real frequency. For substantial plasma flow ($M_A > 0.1$) the higher n modes are suppressed for $n > 8$. The lower n pick up a substantial real frequency contribution from the Doppler shift with a roughly linear dependence, $\omega \sim V_0$.

In Fig. 3 we illustrate three radial wave structures of the n=5 eigenmode for three different plasma flow velocity and magnetopause boundary layer thickness. $\bar{x} = -0.5$ corresponds to the bow shock position and $\bar{x} = 0.5$ the magnetopause position. The dotted and dashed lines correspond to the real and imaginary part of the eigenfunctions of $\delta B_{||}$, respectively. In all of these three cases, the real frequency is negative (same sign as diamagnetic drift frequency). This means that if the real part of the eigenfunction leads the imaginary part, then the mode travels to the left (phase velocity is negative). Conversely if the imaginary part leads the real part, the wave travels to the right.

For a sharp magnetopause with zero layer width ($\Delta \to 0, V_0 = 0, \bar{\omega} = (0, 0.73)$, the eigenfunction (the top panel in Fig. 3) is a standing wave. However, for a more realistic magnetopause gradient ($\Delta = 0.05, M_A = 0, \bar{\omega} = (-0.1, 0.81)$), the eigenfunction (the middle panel in Fig. 3) is complex and the real and imaginary parts of the eigenfunction are not in phase. Near the magnetopause where τ_{MHD} is small, the imaginary part of τ dominates over the real part and leads to a phase shift in the real and imaginary parts of the eigenfunction. Because there is a real frequency associated with the wave, the structure slowly propagates

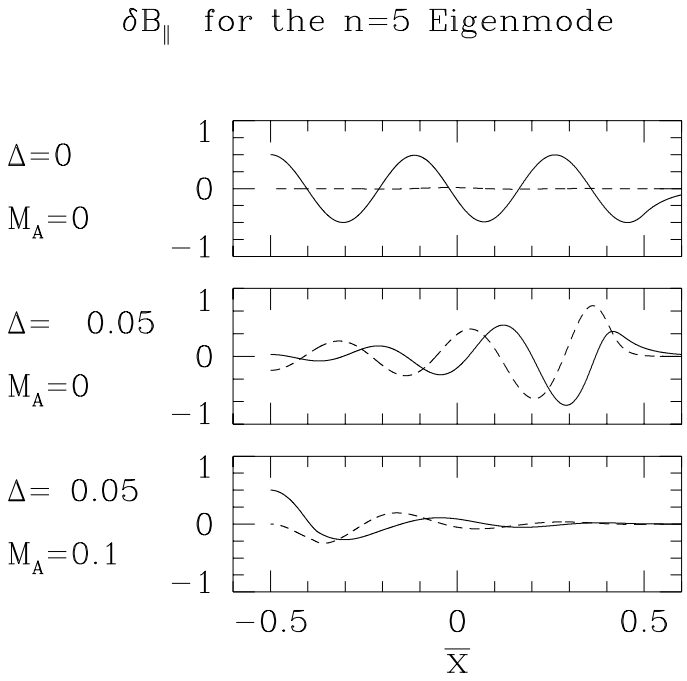

FIG. 3. Three radial wave structures of $\delta B_{||}$ (real: solid lines, imag: dashed lines) for the n=5 eigenmode for three different plasma flow velocity and magnetopause boundary layer thickness corresponding to three different points on the curve shown in Fig. 2. Notice that the density gradients and bulk flow strongly modify the mode structure. Note that n indicates the number of nodes of the eigenfunction.

as it grows. The wave amplitude is largest near the magnetopause. To understand why the eigenmode is skewed we consider the local dispersion relation in the magnetosheath region far away from the magnetopause boundary. The mode has largest growth with $k_{||} > k_y$ and $\omega < k_{||}V_A$ so that $\tau k_x^2 \approx -\sigma k_{||}$. Because diamagnetic drift effects are unimportant and $\omega_r \ll \omega_i$, $|\tau_r| \gg |\tau_i|$ and we have $k_x \approx \pm k_0(1+i\delta)$ where $k_0 = \sqrt{-\sigma k_{||}^2/\tau_r}$ and $\delta = -\tau_i/2\tau_r$. For unstable modes with $|\omega/k_{||}v_{th}| \ll 1$, $\tau_r < 0$ and $\tau_i \approx -\sqrt{\pi}(\beta_\perp T_\perp/T_{||})\omega_r/k_{||}v_{th}$. For $\omega_r < 0$, $\tau_i > 0$ and $\delta > 0$. By inspection of the eigenfunction, $k_{xr} < 0$ (the imaginary part of the eigenfunction leads the real part) and hence the eigenfunction will have the spatial behavior, $\exp(-ik_0x + \delta k_0 x)$, which increases in amplitude in the positive x direction.

Because the real frequency is a consequence of the diamagnetic drift at the magnetopause, this growth can be interpreted to result from coupling of the wave with the diamagnetic drift associated with the pressure gradient. The diamagnetic drift causes the waves to drift with phase velocity toward the magnetopause boundary. As a result, the waves pile up against the magnetopause and the wave amplitude is enhanced. Although the diamagnetic drift is only large near the magnetopause, its effects are globally transmitted throughout the entire spatial domain leading to a slowly propagating mirror mode with real frequency.

When the plasma flow is included ($\Delta = 0.05, M_A = 0.1, \bar{\omega} = (-0.2, 0.7)$) the real frequency of the mode is some combination of an averaged $\mathbf{k}\cdot\mathbf{V}_0$ and ω_*. The real and imaginary parts of the eigenfunction (the bottom panel in Fig. 3) are out of phase which indicates that the wave phase velocity is in the flow direction. The solutions are skewed toward the bow shock. To physically understand the origin of the relatively larger real frequency, we note that the mode is most unstable when the arguments of the Z-functions $(\omega - \mathbf{k}\cdot\mathbf{V}_0)$ is small so that $\omega - \mathbf{k}\cdot\mathbf{V}_0 \simeq 0$ and the wave has a real frequency close to an average value of $\mathbf{k}\cdot\mathbf{V}_0$. The behavior of the amplitude can be understood by considering $|(\omega - \mathbf{k}\cdot\mathbf{V}_0)/k_{||}v_{th}| \ll 1$. In this case $\tau_i \approx -\sqrt{\pi}(\beta_\perp T_\perp/T_{||})(\omega_r - \mathbf{k}\cdot\mathbf{V}_0)/k_{||}v_{th}$. The real part of the n=5 mode local wavevector varies between -5 and -10 over most of the domain so that $\mathbf{k}\cdot\mathbf{V}_0 \approx -(0.5 - 1.0)$ whereas $\omega_r = -0.2$ so that $\tau_i < 0$. For unstable modes $\tau_r < 0$, then $\delta = -\tau_i/2\tau_r < 0$ and $k_0 > 0$. Hence the mode has a spatial behavior, $\exp(-ik_0x + \delta k_0 x)$ so that the mode decays with increasing values of x. Physically, because the mirror mode propagates in the same direction as the flow but with a slower phase velocity, the mode will propagate toward the bow shock direction in the plasma moving frame. As the mode propagates toward the bow shock, its amplitude is enhanced by additional pressure anisotropy free energy and its energy accumulates near the the bow shock boundary because of the reflecting boundary condition there.

In general, the actual wave structure at the magnetopause will consist of a large number of modes because the growth rates for the modes are approximately the same (see Fig. 2). It is expected that finite Larmor radius effects will suppress the modes with sufficiently

large k_x and that there will be some range of n with maximum growth. We expect that the observations will consist of many such modes with different k_x. As a result, there will be substantial beating between the waves leading to mirror mode wave structures with shorter spatial scale which would be comparable with the scales that are observed. The theory predicts a skew in the amplitude toward the magnetopause for small radial plasma flow and a skew toward the magnetosheath for large radial plasma flow. These are predictions from the theory that can be carefully compared with the observations in order to determine whether further refinements might be required for the theory.

V. CONCLUSIONS

In this paper we have presented an eigenmode analysis of the global mirror mode at the magnetopause using the kinetic-MHD model which accounts for both kinetic effects and global effects due to background gradients. The analysis demonstrates that:

- magnetopause gradients and plasma flow lead to a substantial real part of the eigenfrequency for the global mirror modes which is on the order of a combination of the Doppler shift frequency associated with plasma flow and diamagnetic drift frequencies,

- pressure and density gradients at the magnetopause modify the wave structure because of diamagnetic drift effects. The real frequency associated with the diamagnetic drift frequency provides a wave phase velocity in the direction of the magnetopause so that wave energy accumulates against the magnetopause boundary and the amplitude is skewed in that direction.

- plasma flow also gives rise to a real phase velocity, but the phase velocity is smaller than the flow velocity. As a result, the wave amplitude is increased in the wake of the plasma flow and piles up against the bow shock boundary and is skewed in that direction.

- boundary conditions are important because they impose restrictions that determine the global solution far away from the boundary and determine how the waves propagate within the region of instability,
- the kinetic-MHD formalism is useful when it is important to consider both global scale gradients and kinetic effects.

We want to reiterate that the real frequency that these modes exhibit has important consequences for magnetopause transport because efficient mode conversion to kinetic Alfvén waves can occur at the magnetopause boundary–particularly if the magnetic field rotates so that the Alfvén resonance frequency goes through a minimum. The wave energy is funneled to small scales (the order of the ion gyroradius) which can lead to efficient cross field transport.

One obvious direction for future consideration is an extension to obtain two-dimensional mirror mode solutions based on a two-dimensional magnetosheath-magnetopause configuration which includes the effects of curvature. Another important area for further consideration is coupling between the compressional and transverse components of the perturbed magnetic field which becomes essential near the shear Alfvén and slow magnetosonic resonances. Because these modes have a real frequency, they can couple strongly with the kinetic Alfvén wave near the location where the real frequency matches the local shear Alfvén resonance frequency which will occur if the background magnetic field rotates. Such coupling could lead to enhanced particle transport across the magnetopause boundary layer.

APPENDIX: INTEGRALS OVER PRODUCTS OF BESSEL FUNCTIONS

In the kinetic-MHD equations, the fields are multiplied by J_0 and J_1 so that integrals over the product $J_0 J_1$ are frequently encountered. Integrals of this type may be evaluated through differentiation on the well known integral 6.633.1 from [26]

$$\mathcal{I}_1(\alpha,\lambda) \equiv \int_0^\infty \exp(-\alpha\xi^2)[J_0(\lambda\xi)]^2 \xi d\xi = \frac{1}{2\alpha}\exp(-\lambda^2/2\alpha) I_0(\lambda^2/2\alpha) \tag{A1}$$

where I_0 is the modified Bessel function.

Kinetic effects for the core plasma involve two integrals

$$\mathcal{I}_2 \equiv \int_0^\infty \exp(-\xi^2) J_0(\lambda\xi) J_1(\lambda\xi) \xi^2 d\xi \tag{A2}$$

$$\mathcal{I}_3 \equiv \int_0^\infty \exp(-\xi^2) J_0(\lambda\xi) J_1(\lambda\xi) \xi^4 d\xi \tag{A3}$$

$$\mathcal{I}_5 \equiv \int_0^\infty \exp(-\xi^2) J_0(\lambda\xi) J_1(\lambda\xi) \xi^6 d\xi \tag{A4}$$

Using the relationship

$$\frac{\partial J_0(z)}{\partial z} = -J_1(z) \tag{A5}$$

we find that

$$\mathcal{I}_2 = -\frac{1}{2}\frac{\partial \mathcal{I}_1}{\partial \lambda}\bigg|_{\alpha=1} \tag{A6}$$

$$\mathcal{I}_3 = \frac{1}{2}\frac{\partial^2 \mathcal{I}_1}{\partial \lambda \partial \alpha}\bigg|_{\alpha=1} \tag{A7}$$

$$\mathcal{I}_5 = -\frac{1}{2}\frac{\partial^3 \mathcal{I}_1}{\partial \lambda \partial \alpha^2}\bigg|_{\alpha=1}. \tag{A8}$$

We find through differentiation using the rule

$$2\frac{\partial I_n(z)}{\partial z} = I_{n-1}(z) + I_{n+1}(z) \tag{A9}$$

and

$$\frac{2n}{z} I_n(z) = I_{n-1}(z) - I_{n+1}(z) \tag{A10}$$

and with the auxiliary definition

$$\Gamma_n(z) = \exp(-z) I_n(z) \tag{A11}$$

that

$$\mathcal{I}_2 = \frac{\lambda}{4}[\Gamma_0(\lambda^2/2) - \Gamma_1(\lambda^2/2)] \tag{A12}$$

$$\mathcal{I}_3 = \frac{\lambda}{2}\left\{[1-\lambda^2/2]\Gamma_0 - [1-\lambda^2]\Gamma_1/2\right\} \tag{A13}$$

$$\mathcal{I}_5 = \frac{3\lambda}{2}\left\{[1-11\lambda^2/12+\lambda^4/6]\Gamma_0 - [1-9\lambda^2/4+\lambda^4/2]\Gamma_1/3\right\} \tag{A14}$$

The limiting forms of these expressions are of interest. The power series representations (in λ) of these functions is

$$\mathcal{I}_2 = \frac{\lambda}{4}(1 - 3\lambda^2/4 + 5\lambda^4/16 + ... \tag{A15}$$

$$\mathcal{I}_3 = \frac{\lambda}{2}(1 - 9\lambda^2/8 + 5\lambda^4/8 + ... \tag{A16}$$

$$\mathcal{I}_5 = \frac{3\lambda}{2}(1 - 3\lambda^2/2 + 83\lambda^4/48 + ... \tag{A17}$$

The asymptotic expansions for large λ are

$$\mathcal{I}_2 \sim \frac{1}{4\sqrt{\pi}\lambda^2} \tag{A18}$$

$$\mathcal{I}_3 \sim -\frac{7}{8\sqrt{\pi}\lambda^2} \tag{A19}$$

$$\mathcal{I}_5 \sim \frac{3}{16\sqrt{\pi}\lambda^2} \tag{A20}$$

ACKNOWLEDGMENTS

This work is supported by the DoE Contract No. DE-AC02-76-CHO3073 and NSF grant ATM-9523331.

REFERENCES

[1] C. P. Price, D. W. Swift, and L. C. Lee, J. Geophys. Res. **91**, 101 (1986).

[2] R. E. Denton *et al.*, J. Geophys. Res. **100**, 5665 (1995).

[3] S. P. Gary, J. Geophys. Res. **97**, 8519 (1992).

[4] B. J. Anderson, S. A. Fuselier, S. P. Gary, and R. E. Denton, J. Geophys. Res. **99**, 5877 (1994).

[5] P. Song, C. T. Russell, and M. F. Thomsen, J. Geophys. Res. **97**, 8295 (1992).

[6] P. Song, C. T. Russell, and C. Y. Huang, J. Geophys. Res. **98**, 5907 (1993).

[7] P. Song *et al.*, J. Geophys. Res. **98**, 187 (1993).

[8] N. Omidi and D. Winske, J. Geophys. Res. **100**, 11,935 (1995).

[9] S. P. Gary, M. E. McKean, and D. Winske, J. Geophys. Res. **98**, 3963 (1993).

[10] A. Hasegawa and K. Mima, Phys. Rev. Lett. **36**, 1362 (1978).

[11] L. C. Lee, J. R. Johnson, and Z. W. Ma, J. Geophys. Res. **99**, 17405 (1994).

[12] J. R. Johnson and C. Z. Cheng, EOS Trans. AGU **76**, 516 (1995).

[13] J. R. Johnson and C. Z. Cheng, EOS Trans. AGU **76**, 252 (1995).

[14] B. J. Anderson, S. A. Fuselier, and D. Murr, Geophys. Res. Lett. **18**, 1955 (1991).

[15] G. Paschmann, W. Baumjohann, N. Sckopke, and T.-D. Phan, J. Geophys. Res. **98**, 13,409 (1993).

[16] A. Hasegawa, Phys. Fluids **12**, 2642 (1969).

[17] S. P. Gary, S. A. Fuselier, and B. J. Anderson, J. Geophys. Res. **98**, 1481 (1993).

[18] S. P. Gary *et al.*, Geophys. Res. Lett. **20**, 1767 (1993).

[19] S. P. Gary and D. Winske, J. Geophys. Res. **98**, 9171 (1993).

[20] C. Z. Cheng, J. Geophys. Res. **96**, 21,159 (1991).

[21] C. Z. Cheng, Geophys. Res. Lett. **22**, 2401 (1995).

[22] D. J. Southwood and M. G. Kivelson, J. Geophys. Res. **98**, 9181 (1993).

[23] E. A. Frieman and L. Chen, Phys. Fluids **25**, 502 (1982).

[24] L. Chen and A. Hasegawa, J. Geophys. Res. **79**, 1024 (1974).

[25] D. H. Fairfield, J. Geophys. Res. **75**, 6700 (1971).

[26] I. S. Gradshteyn and I. M. Ryzhik, *Table of Integrals, Series and Products* (Academic Press, London, 1963).